JGR Atmospheres

RESEARCH ARTICLE
10.1029/2019JD031726

Special Section:
Stratospheric aerosol during the post Pinatubo era: processes, interactions, and impact

The Role of the SO_2 Radiative Effect in Sustaining the Volcanic Winter and Soothing the Toba Impact on Climate

Sergey Osipov[1,2], Georgiy Stenchikov[1], Kostas Tsigaridis[3,4], Allegra N. LeGrande[3,4], and Susanne E. Bauer[4]

[1]Physical Science and Engineering, King Abdullah University of Science and Technology, Thuwal, Saudi Arabia, [2]Atmospheric Chemistry Department, Max Planck Institute for Chemistry, Mainz, Germany, [3]Center for Climate Systems Research, Columbia University, New York, NY, USA, [4]NASA Goddard Institute for Space Studies, New York, NY, USA

Abstract Volcanic eruptions are an important climate driver. The impact of Pinatubo-sized eruptions has been observed and is well constrained. The magnitude and duration of volcanic winter effects after supereruptions such as Toba remain disputed due to disagreement between the strong cooling predicted by models and much milder climate perturbations according to the paleodata. Here we present a reevaluated climate impact of a Toba-sized supereruption based on up-to-date GISS ModelE simulations. In this study, we account for all known primary mechanisms that govern the evolution of the volcanic plume and their nonlinear interactions. The SO_2 radiative effects are evaluated for the first time in coupled climate simulations with the interactive atmospheric chemistry module. We found that SO_2 effects on photochemistry, dynamics, and radiative forcing are especially prominent. Due to strong absorption in ultraviolet, SO_2 feedback on photochemistry partially offsets the limiting effect associated with aerosol microphysical processes. SO_2 greenhouse warming soothes the radiative cooling exerted by sulfate aerosols. SO_2 absorption in the shortwave and longwave causes radiative heating and lofting of the volcanic plume, and boosts the efficiency of SO_2 impact on photochemistry. Our analysis shows that SO_2 lifetime and magnitude of effects scale up and increase with the amount of emitted material. For a Pinatubo-sized eruption, SO_2 feedbacks on chemistry and dynamics are relevant only during the initial stage of the volcanic plume evolution, while local SO_2 concentrations are high. For a Toba-sized eruption, SO_2 effects are as important as sulfate aerosols and produce a less extreme volcanic winter.

Key Points:
- SO_2 inhibits production of sulfate aerosols and sustains volcanic winter effects
- SO_2 greenhouse warming partially offsets the aerosols radiative cooling
- SO_2 enhances lofting of the volcanic plume

Correspondence to:
S. Osipov,
Sergey.Osipov@mpic.de;
Sergey.Osipov@kaust.edu.sa

Citation:
Osipov, S., Stenchikov, G., Tsigaridis, K., LeGrande, A. N., & Bauer, S. E. (2020). The role of the SO_2 radiative effect in sustaining the volcanic winter and soothing the Toba impact on climate. *Journal of Geophysical Research: Atmospheres*, *125*, e2019JD031726. https://doi.org/10.1029/2019JD031726

Received 24 SEP 2019
Accepted 20 DEC 2019
Accepted article online 3 JAN 2020

1. Introduction

The largest stratovolcanic eruptions, known as "supereruptions," have the potential to alter Earth's climate significantly. The Toba eruption in Sumatra about 74,000 years ago is a prominent example. The extreme cooling during the posteruption "volcanic winter" is the key component that initially drew attention to the Toba eruption and linked it to two major hypotheses: the human genetic bottleneck (Ambrose, 1998) and the accelerated shift to glacial conditions (Rampino & Self, 1992). Since then these theories have been tested by models and available observations, but the conclusions remain disputed and controversial. While numerical simulations do predict climate to switch to a colder state for several years after the Toba eruption, they do not initiate glaciation (Robock et al., 2009; Timmreck et al., 2012). In the literature (Yost et al., 2018), the maximum simulated global mean cooling anomalies range from severe −18 °C to a relatively mild −3.5 °C, which is only 5 times larger than the recent cooling observed after the 1991 Pinatubo eruption (Stenchikov et al., 2009). Paleodata even suggest that the climate of East Africa was not substantially affected at all (Lane et al., 2013; Oppenheimer, 2002; Smith et al., 2018; Yost et al., 2018). Thus, the assumption itself regarding extreme cooling after the Toba eruption may not be valid. The wide range of cooling estimates and discrepancies between simulations and observations indicate that previous modeling efforts likely did not consider some fundamental physical and chemical processes. The scientific community proposed several such mechanisms that might govern the evolution of the volcanic supereruption plume and modulate climate impact (Kondratyev et al., 1986). The comprehensive intercomparison of these mechanisms is a primary focus of this work.

Table 1
Previous Toba Modeling Studies and the Main Mechanisms and Feedbacks Included (Binary 1) and Excluded (Binary 0) in the Simulations

Modeling study	Aerosol microphysics (**x**xxx)	Aerosols feedback on chemistry (x**x**xx)/ dynamics	SO_2 feedback on chemistry (xx**x**x)/ dynamics (xxx**x**)	Coupled atmos-ocean
Bekki et al. (1996) 300× Pinatubo	1	0/0	1/1	0
Robock et al. (2009) 300× Pinatubo	0	1/0	0/0	1
Timmreck et al. (2010) 87.5× Pinatubo	1	1/—	0/0	—
Jones et al. (2005) 100× Pinatubo	0	0/0	0/0	1
English et al. (2013) 10–100× Pinatubo	1	0/0	0/0	0
This study 100× Pinatubo	1	1/1	1/1	1

Note. Four of these mechanisms are diagnosed in this study (and selectively switched off one by one in the sensitivity experiments) and are indicated by the bold letter in the binary "xxxx" mask in the column headers. The remaining two mechanisms are not diagnosed, that is, we perform only the coupled atmosphere-ocean simulations, and aerosols feedback on radiative transfer and dynamics is always active. All studies except Jones et al. (2005) simulated interactive chemistry with the sulfate cycle. Robock et al. (2009) refers to the interactive chemistry ModelE setup. Timmreck et al. (2010) used a two-step approach. Sulfate aerosol evolution was first evaluated in the atmospheric model (ECHAM/HAM) with prescribed SST, and then climate impact was computed in the coupled atmosphere-ocean ECHAM5-MPIOM model with prescribed sulfate aerosols forcing. Bekki et al. (1996) used the interactive 2-D model. 1× Pinatubo emission of SO_2 is assumed to be 20 Mt for simplicity here, since there is no consensus in the literature on the exact amount.

The first estimates of climate forcing induced by supereruptions were based on simple extrapolation of the forcing and emitted mass from smaller but climate-relevant eruption such as Mount Pinatubo in 1991 in the Philippines (Robock, 2000; Stenchikov et al., 1998). Many separate modeling efforts using atmospheric chemistry modules indicated that climate forcing and temperature anomalies do not scale linearly with the amount of SO_2 emissions (Pinto et al., 1989). For example, aerosol microphysics is an important limiting mechanism that confines volcanic forcing and contributes to less than linear scaling. The coagulation of sulfate aerosol particles (driven by their high concentration) reduces the aerosols lifetime and the efficiency of radiative cooling (Lacis et al., 1992). The increase of effective radius and shift toward larger particles results in a rapid gravitational fallout of droplets (Timmreck et al., 2010) and causes redistribution of the spectral optical depth, which decreases in visible and increases in near-infrared and longwave (English et al., 2013).

Ozone photolysis is a primary source of OH, which drives SO_2 oxidation and modulates the rate of SO_2 decay and sulfate aerosols production (LeGrande et al., 2016). Thus any perturbation of photochemistry is potentially another key mechanism with control over the "volcanic winter" effect. Aerosols (Dickerson et al., 1997) and SO_2 (Bekki, 1995; Bekki et al., 1996) are the two radiative agents capable of reducing actinic flux and slowing down photochemical conversion of SO_2 to sulfate aerosols. These mechanisms are nonlinear, since the depletion and production rates of the agents themselves are affected by their concentration.

Another implication of SO_2 being optically active is its effect on dynamics and volcanic plume evolution. SO_2 heating rates are positive (below the ozone maximum) within the plume (Lary et al., 1994; Zhong et al., 1996) and cause lofting. Additionally, SO_2 is a greenhouse gas and counteracts volcanic aerosol radiative cooling (Ward, 2009). This is the first study to include all of these SO_2 effects on chemistry, dynamics, and associated radiative forcing, in a 3-D general circulation model with interactive chemistry enabled.

Previous research showed that these specific mechanisms can individually change the duration and magnitude of volcanic forcing drastically. The resulting combined effect, however, remains unclear, since competing processes tend to both prolong and shorten the volcanic winter. Table 1 summarizes previous

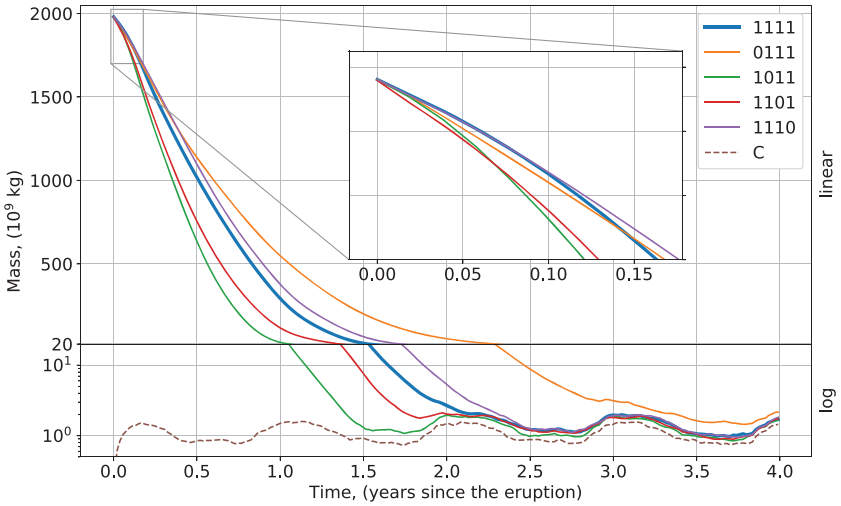

Figure 1. The instantaneous weekly globally integrated SO_2 mass for the reference experiment (1111, all feedback are on), sensitivity experiments (xxxx, one of the feedback is switched off), and control experiment (C, does not include volcanic emissions). In the sensitivity experiments the following mechanisms are switched off one by one: aerosols microphysics (0111); feedback on photochemistry due to aerosols (1011) and SO_2 (1101); and SO_2 feedback on dynamics (1110). The linear-log threshold is set at 20 Mt or 1% of the emission mass (2,000 Mt).

studies that quantified Toba's impact and highlights which mechanisms were present and absent in each of the studies.

In this work our first goal is to provide an updated estimate of Toba's impact on climate, based upon comprehensive and realistic numerical simulations that account for all recently proposed primary mechanisms (Table 1) and their nonlinear interactions. The second goal is to highlight the importance of SO_2 effects and to study their scaling with the amount of emitted material.

Table 2
The Characteristic Time Scales of SO_2 Oxidation and SO_4 Production for the Reference Experiment (1111, All Feedback Are on) and Sensitivity Experiments (xxxx, One of the Feedback Is Switched Off)

Diagnostic	1111	0111	1011	1101	1110
SO_2 time to 50% of the emission mass, (days)	189	224	133	147	203
Change due to the feedback, (%)		−15.6	42.1	28.6	−6.9
SO_2 time to 1% of the emission mass, (days)	560	840	385	497	630
Change due to the feedback, (%)		−33.3	45.5	12.7	−11.1
SO_2 time to background level, (days)	756	1358	525	700	875
Change due to the feedback, (%)		−44.3	44.0	8.0	−13.6
SO_2 mass-time integral, (2,000 Mt * 1 day)	209	264	145	165	228
Change due to the feedback, (%)		−20.9	44.4	26.5	−8.4
SO_4 time to maximum value, (days)	322	560	280	287	329
Change due to the feedback, (%)		−42.5	12.2	12.2	−2.1
SO_4 mass-time integral, (2000 Mt * 96/64 * 1 day)	357	623	359	344	399
Change due to the feedback, (%)		−42.8	−0.6	3.6	−10.6

Note. In the sensitivity experiments the following mechanisms are switched off one by one: aerosols microphysics (0111); feedback on photochemistry due to aerosols (1011) and SO_2 (1101); and SO_2 feedback on dynamics (1110). The second line in each row shows the contribution of the switched-off feedback and is represented by the relative change of the diagnostic in the reference simulation relative to the sensitivity simulation. The SO_2 mass is considered at background level, when the anomaly with respect to the control run is below 0.75 Mt.

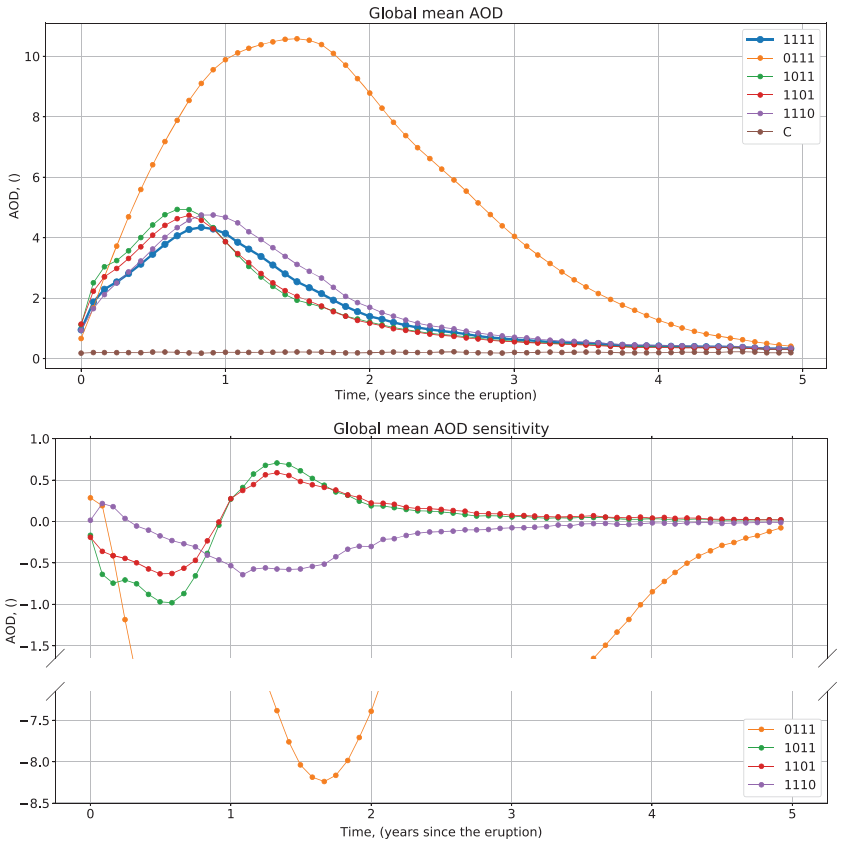

Figure 2. The monthly average global mean aerosols optical depth (AOD) at 550 nm and contribution of the individual feedback. Top panel shows AOD for the reference experiment (1111, all feedback are on); sensitivity experiments (xxxx, one of the feedback is switched off); and control experiment (C, does not include volcanic emissions). The bottom panel shows AOD changes due to individual mechanisms, represented by the difference between reference and sensitivity simulations. In sensitivity experiments the following mechanisms are switched off one by one: aerosols microphysics (0111); feedback on photochemistry due to aerosols (1011) and SO_2 (1101); and SO_2 feedback on dynamics (1110).

2. Experimental Setup

In this work, we analyze volcanic plume evolution and impact on climate primarily using the Goddard Institute for Space Studies (GISS) Earth system model (ModelE) simulations. However, the complex and nonlinear interplay of the numerous feedbacks makes interpretation of results complicated. Stand-alone models were developed and employed to supplement analysis and discussion of ModelE simulations. These auxiliary tools are introduced throughout the text and described in Appendix A. Below we highlight the details specific to this study, while Schmidt et al. (2006) provides a complete description of ModelE.

To simulate volcanic plume evolution, ModelE includes fully interactive chemistry related to ozone (Shindell et al., 2013) and sulfate (Koch et al., 1999, 2006). The sulfate chemistry scheme provides gas-phase conversion of SO_2 to H_2SO_4 and the aqueous sulfate production rate for liquid clouds, as well as H_2SO_4 concentration for the aerosol microphysics scheme. The eruption of Toba is modeled by instantaneous injection of 2000 Mt of SO_2 (100× Pinatubo; Guo et al., 2004) on 1 January. Emitted SO_2 is distributed with the constant mixing ratio of 10.9 ppmv in the 20°S to 20°N equatorial belt between 10 and 50 hPa. Actinic flux and photolysis rates are calculated in the presence of cloud and aerosol layers, using the accurate and efficient Fast-J scheme (Wild et al., 2000).

Due to the large magnitude of volcanic atmospheric forcing, ocean-atmosphere interaction plays a paramount role. To properly capture climate response, we used a coupled version of the GISS-E2.1 version of ModelE with the Russel interactive ocean model (Russell et al., 1995; Schmidt et al., 2014) on a 1.25° × 1° grid, coupled to the atmospheric model on a 2° × 2.5° grid, each with 40 vertical layers. The ocean was

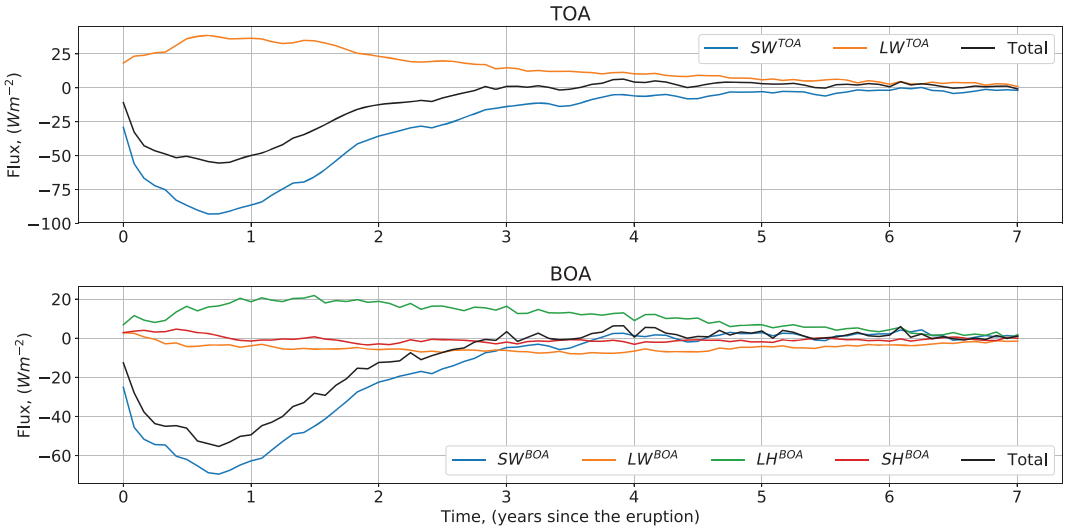

Figure 3. Monthly average global mean energy balance anomalies of the reference simulation (1111, with the SO_2 emissions) with respect to the control run (C, without SO_2 emissions). Top panel shows TOA SW, LW, and total (SW+LW) net (downward minus upward) flux anomalies. Bottom panel shows BOA SW, LW, latent (LH), sensible (SH), and total (SW+LW+LH+SH) net flux anomalies. The fluxes sign choice follows convention, where the downward direction is positive, and a positive value of flux means heating of the system.

preliminary spun up for 3600 years. The model initial conditions are for a 1850 preindustrial atmosphere (ozone and greenhouse gases).

To diagnose the overall effect of a Toba-sized eruption and to separate the contribution of the individual mechanisms, several simulations were performed. The reference simulation is labeled "1111" and includes all major mechanisms listed in Table 1. This simulation is the most comprehensive representation of plume evolution, forcing, and climate response to a Toba-sized volcanic eruption. The control simulation is labeled "C." It is the only volcanically "unperturbed" simulation and does not include volcanic emissions in the stratosphere. This auxiliary simulation complements the reference simulation, provides the magnitude of the natural variability, and allows estimates of the overall volcanic effects (diagnostics such as radiative forcing and temperature response). To assess the contribution and role of individual mechanisms, several additional sensitivity experiments were carried out. One of the mechanisms was selectively switched off in each of these simulations. The setups are labeled "xxxx," where the binary mask shows which feedbacks are turned on (x is 1) or off (x is 0). The mask is also available in Table 1.

Simulations that include aerosol microphysics (1xxx) are based on the Multiconfiguration Aerosol TRacker of mIXing state (MATRIX; Bauer et al., 2008) module. The MATRIX module represents nucleation, condensation, coagulation, internal and external mixing, and cloud-drop activation and provides aerosol particle mass, number concentration, and particle size information for 16 mixed-mode aerosol populations.

Simulations without microphysics (0xxx) use the One-Moment Aerosol implementation (Koch et al., 2006). In this setup, the size distribution of sulfate particles is prescribed and does not evolve. The purpose of this simulation is to provide a proxy to the previous research, where this assumption was made routinely. Thus, the size parameters (effective radius $r_{\text{eff}} = 0.5$ μm and effective variance $\sigma_{\text{eff}} = 0.35$, similar to Robock et al., 2009) in this simulation were chosen according to the Pinatubo eruption, which is characterized by smaller particle sizes compared to Toba.

By default, aerosols in ModelE are coupled to a radiation module (dynamics) and actinic flux calculations (interactive chemistry). We diagnose only aerosols feedback on chemistry and deactivate it in the x0xx simulation. Aerosols feedback on radiative transfer and dynamics is always active in all of the setups.

The strength of SO_2 absorption in ultraviolet (UV) is especially pronounced at the concentrations characteristic for a supereruption (1–10 ppmv). The spectral dependence of SO_2 UV absorption cross section is similar to that of ozone (Figures A1 and A2). To account for SO_2 UV optical properties in simulations (xx1x), the Fast-J and actinic flux modules were updated and validated against the stand-alone line-by-line radiative

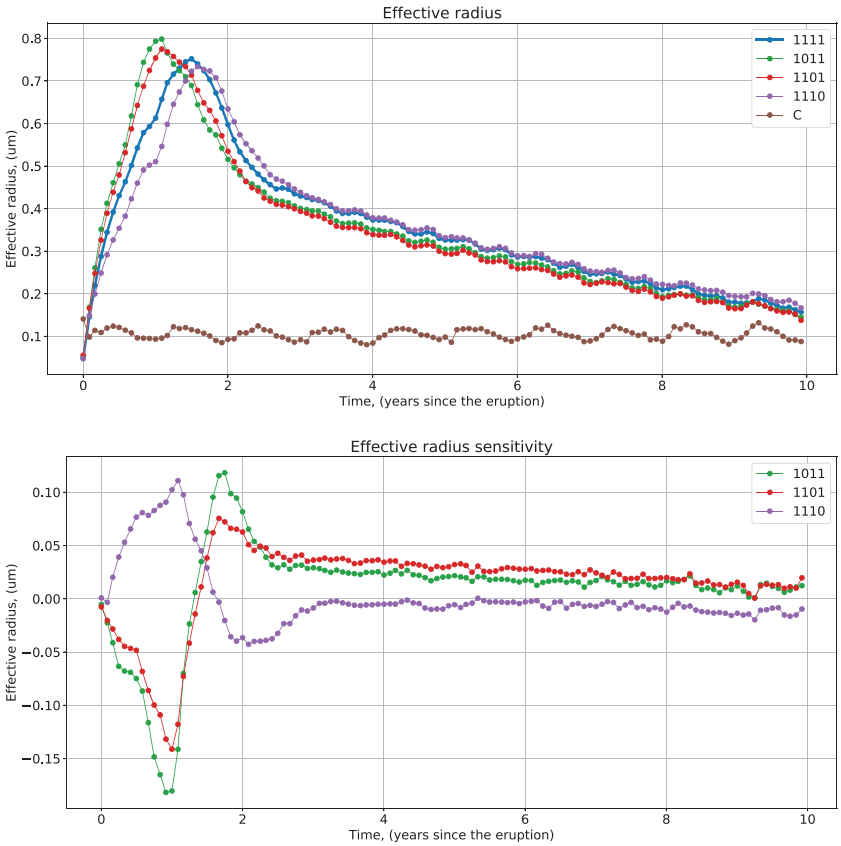

Figure 4. Same as Figure 2 but for the effective radius. The simulation without microphysics (0xxx) is not diagnosed due to prescribed aerosols size distribution. The second moment of the size distribution has been used as an additional weight for the averaging of the effective radius.

transfer simulations. SO_2 feedback on OH chemistry is always active in all of the setups. SO_2 is also a greenhouse gas and absorbs in longwave (LW). SO_2 radiative forcing and heating rates are computed in the LW radiation module (xxx1 simulations) and coupled to the dynamical core but ignored in shortwave (SW). In section 3.4 we use the column model to show that SO_2 radiative forcing in SW is only a small fraction of the LW forcing and can be ignored.

3. Results

The discussion of the results is focused on the three cornerstones that define the Toba impact: sulfate photochemistry, radiative forcing of both gaseous SO_2 and sulfate aerosols, and climate response. In section 3.1, we analyze the oxidation of volcanic SO_2 and gas-to-particle conversion rates, as well as the characteristic time scales necessary for reaching equilibrium. We also explain how the feedbacks (listed in Table 1) affect these processes. In section 3.2 we discuss the optical properties, size distribution, and radiative forcings. Sulfate aerosols are the primary radiative agent with the largest contribution to radiative forcing. However, SO_2 gas is also optically active and partially offsets sulfate cooling. The lifetime of each modulates the resulting total radiative forcing. Aerosol size distribution is another key parameter that controls the aerosols spectral optical depth, lifetime, and thus the forcing. The role of individual mechanisms in modulating the resulting radiative forcing is discussed in section 3.2. Climate response is analyzed in section 3.3. In section 3.4 we study the scaling of SO_2 effects and estimate the threshold value of volcanic emissions below which they can be neglected.

3.1. Temporal Evolution of SO_2 Oxidation

According to the reference experiment (1111), the globally integrated SO_2 mass after the eruption remains elevated above the background level for just over 2 years (756 days, Figure 1). The SO_2 mass is considered at background level, when the anomaly with respect to the control run is below 0.75 Mt. Individually, the

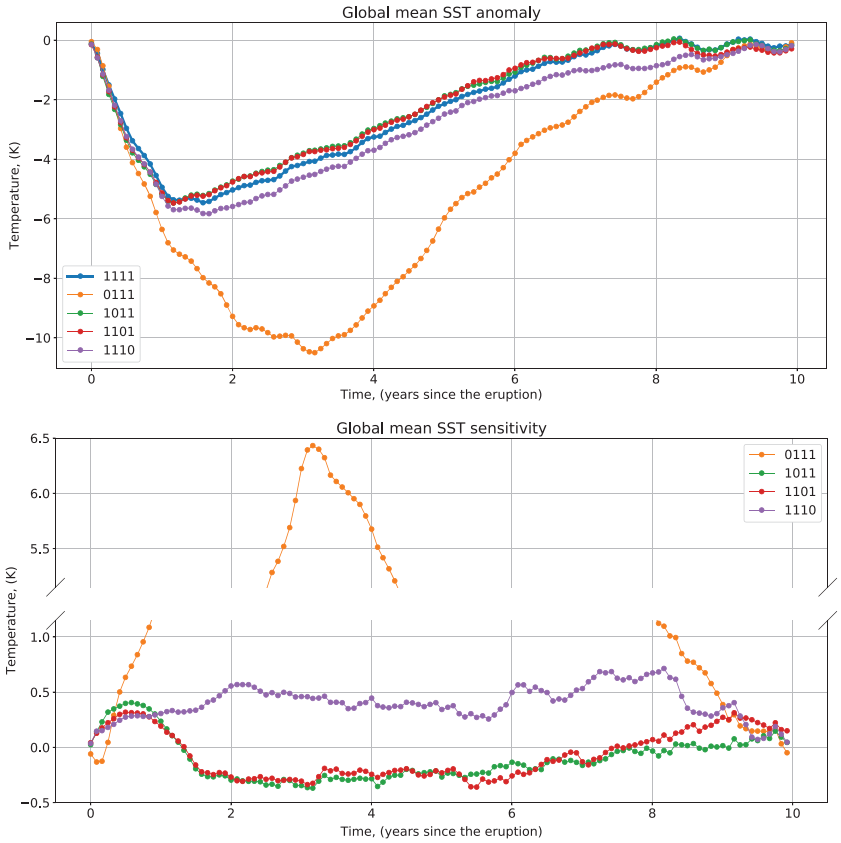

Figure 5. Monthly averaged global mean sea surface temperature (SST) anomaly and contribution of individual feedbacks. Top panel shows the SST anomaly between the perturbed (xxxx, with SO_2 emissions) and control (C, without SO_2 emissions) simulations. Bottom panel shows SST changes due to individual mechanisms represented by the difference between reference (1111, all feedbacks) and sensitivity simulations. In the sensitivity experiments the following mechanisms are switched off one by one: aerosols microphysics (0111); feedback on photochemistry due to aerosols (1011) and SO_2 (1101); and SO_2 feedback on dynamics (1110).

specific feedbacks tend to prolong and to shorten SO_2 lifetime as summarized in Table 2. The largest increase in time necessary for SO_2 to return to the background level (44%) is due to the aerosols effect on chemistry (x1xx). Aerosol microphysics (1xxx) accounts for the largest decrease (44%) due to the shortened sulfate aerosols lifetime. The SO_2 effect on photochemistry (xx1x) is relatively straightforward. It enhances the absorption optical depth in UV (in the Fast-J module), reduces the number of photons that are available for the ozone photolysis, and increases SO_2 equilibration time (time to background level) by 8%. The SO_2 effect on dynamics (xxx1) also has feedback on photochemistry. To explain this result, we have to consider the vertical profiles of the gas species in the stratosphere. Solar and infrared heating, enhanced by SO_2, causes long-term lofting, which pushes the volcanic plume into photochemically more active regions. At these altitudes, the elevated magnitudes of ozone concentration and actinic fluxes accelerate SO_2 oxidation and shorten the equilibration time by 14%. We also highlight that in addition to chemistry, enhanced lofting modifies atmospheric transport and evolution of the volcanic plume, which can be especially important during the initial stage of the eruption.

SO_2 equilibration time is an important diagnostic that shows how long the tracer mass was elevated, but it does not carry information about the magnitude of the climate anomaly it caused. The area under the curve incorporates both parameters (temporal extent and magnitude) and represents a more suitable diagnostic to measure sensitivity and to rank the specific mechanisms. Table 2 provides the relative changes in the mass-time integral $\int_0^T M dt$, where T is the equilibration time and M is the globally integrated mass of the gas species (SO_2 and SO_4). According to this diagnostic, aerosols feedback on photolysis explains 44% increase; 21% decrease is due to aerosol microphysics; and 19% increase is due to combined SO_2 effect on

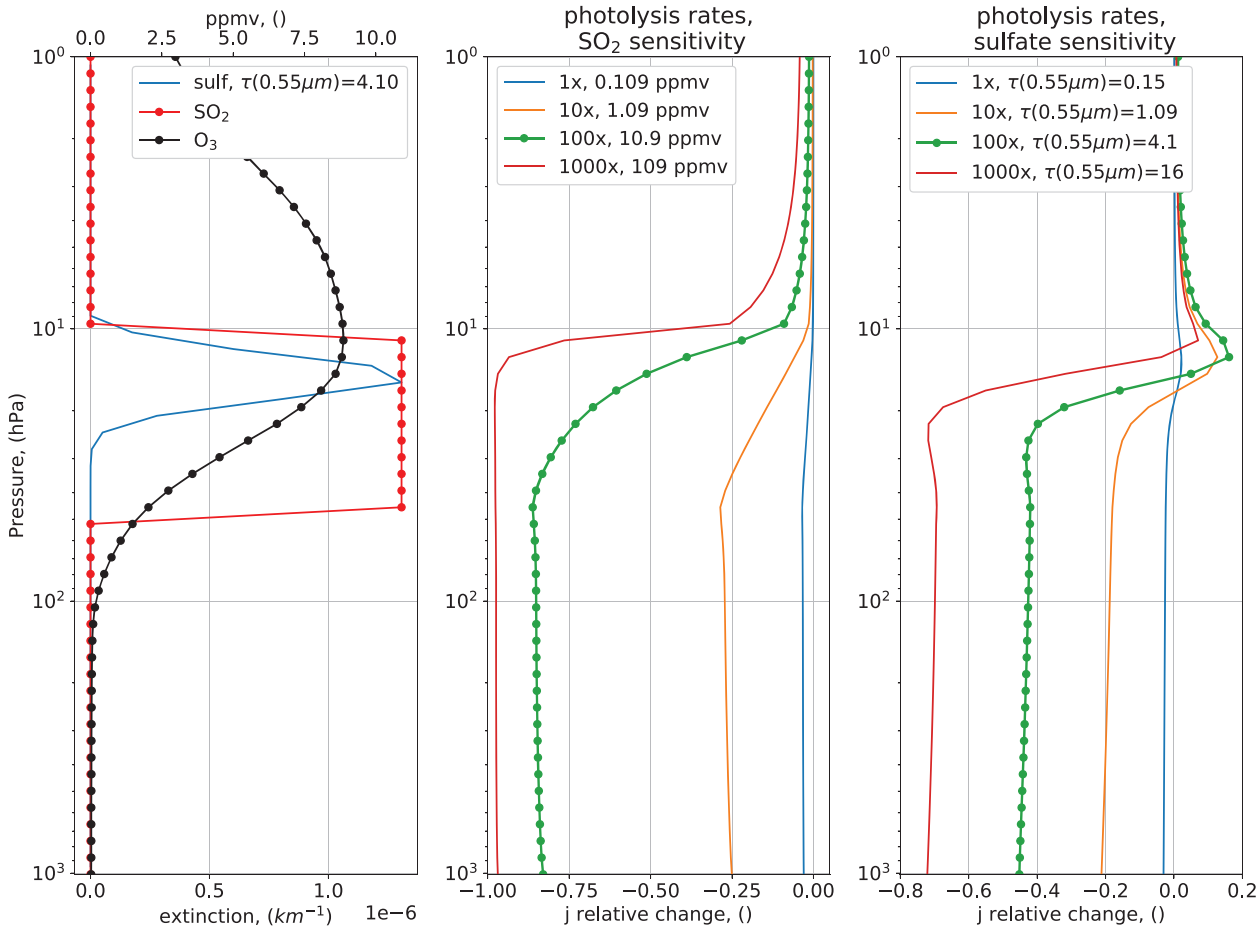

Figure 6. The scaling of SO_2 and sulfate aerosols effects on ozone photolysis rate J(O^1D) computed for equatorial atmosphere using the line-by-line model (LBLRTM coupled to DISORT, see Appendix A). Left panel shows the prescribed vertical profiles of O_3 and SO_2 mixing ratios and aerosol extinction for the 100× Pinatubo (Toba) case. Middle and right panels show the relative change of daylight mean photolysis rate due to SO_2 and aerosols, respectively, for 1×, 10×, 100×, 1,000× Pinatubo cases. The relative change is computed with respect to the reference experiment (with prescribed SO_2 and aerosol optical properties) and sensitivity experiments (only one of the agents is present). For the sulfate aerosols, legends indicate the column integrated optical depth sampled at 0.55 μm. The values of the prescribed sulfate AOD are chosen to represent the maximum globally averaged AOD anomaly. AOD value for the 1× Pinatubo case is obtained from Sato et al. (1993). For the 10× and 100× cases, AOD is obtained from ModelE simulations. For the 1000× case AOD is obtained by extrapolation.

photolysis (27%) and on dynamics (−8%). The temporal evolution of the SO_4 mass is shown in the appendix in Figure A3.

3.2. Radiative Forcing

Sulfate aerosols radiative forcing is the primary driver of volcanic impact on climate. In terms of radiative transfer, forcing is determined by the spectral optical properties of aerosols; and in the case of weakly absorbing sulfate aerosols, mostly by the optical depth in the visible shown in Figure 2. According to the reference experiment (1111), global mean aerosol optical depth (AOD) at 550 nm does not exceed 4.3, reaches the maximum in 11 months, and remains elevated for 6 years. The bottom panel of Figure 2 shows the anomalies due to each mechanism and reveals that aerosol microphysics (1xxx) plays the dominant role. This result is explained by the Mie theory and by the dependence of aerosols optical properties on size distribution, since smaller particles produce larger optical depth per unit mass (in a given range of wavelengths and size distribution parameters). This effect was first identified by Pinto et al. (1989), tested by Timmreck et al. (2010), and stands in our simulations. The contributions of the remaining mechanisms have similar magnitudes (up to 25%) relative to the reference simulation. SO_4 and SO_2 feedback on OH chemistry (through ozone photolysis and water vapor oxidation by O^1D) inhibit sulfate production and thus reduce AOD (mostly due to reduced sulfate mass) before it reaches the maximum. Due to their increased SO_2 lifetime (and thus larger

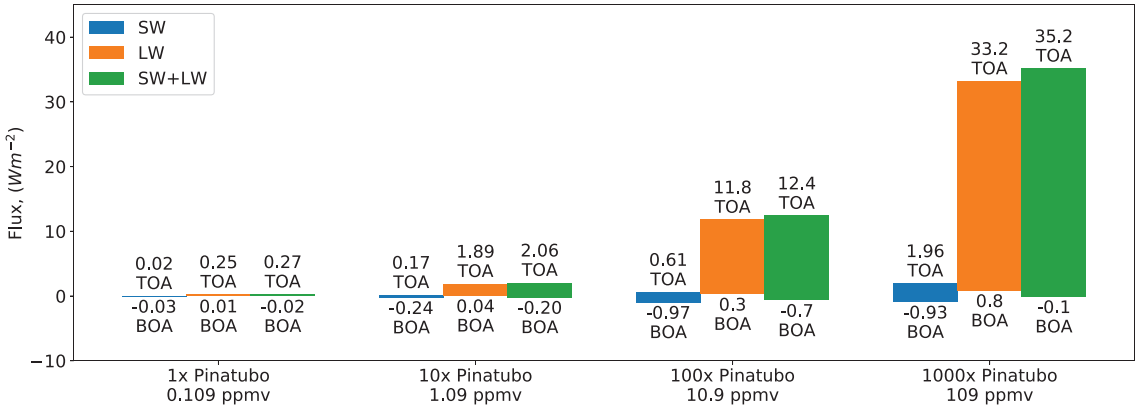

Figure 7. The scaling of SO_2 SW (blue), LW (orange), and total (SW+LW, green), daily mean net radiative forcings computed for a range (1×, 10×, 100×, and 1,000× Pinatubo) of SO_2 volume mixing ratios. The labeled edges of each bar indicate TOA and surface (BOA) radiative forcings. The height of the bar indicates the magnitude of atmospheric absorption due to SO_2. Radiative transfer is calculated using the Rapid Radiative Transfer Model (RRTM, see Appendix A) for equatorial atmosphere. The SW forcing for the 1,000× Pinatubo case (109 ppmv) is computed using the Line-By-Line Radiative Transfer Model (LBLRTM) since the extremely high SO_2 loading requires accurate spectral fluxes in UV. The prescribed vertical profiles of O_3 and SO_2 mixing ratios and aerosol extinction for the 100× Pinatubo (Toba) case are shown in Figure 6.

available mass), these feedback boost AOD after it reaches the maximum. The sign change in AOD difference between reference and sensitivity simulations highlights this result (bottom panel in Figure 2). Thus, the maximum AOD value is reduced and delayed by 2 months and the overall AOD temporal distribution becomes more uniform.

Heating of the plume by SO_2 does not affect the timing of AOD maximum but rather reduces the magnitude of AOD (due to reduced sulfate mass) during the entire aerosols lifetime (except for the initial 3 months). This result is counterintuitive, since SO_2 feedback on dynamics reduces SO_2 lifetime (described in section 3.1) and should (but does not) increase AOD due to larger sulfate mass. To resolve this puzzle, we have to consider the process responsible for the growth of particles and the nonlinear dependence of gravitational settling on particle size. SO_2 feedback on dynamics accelerates the rate of gas-to-particle conversion (due to faster SO_2 oxidation) in the most photochemically active region, which in turn increases the number of nucleating particles and accelerates coagulation, responsible for the growth of sulfate aerosols. This chain eventually leads to faster gravitational removal of the sulfate mass and reduced AOD. A more detailed analysis of the aerosols size distribution is provided later in this section.

Climate response is driven by the perturbations of energy balance shown in Figure 3. The top panel shows overall energy loss by Earth's system at the top of the atmosphere (TOA). According to the reference experiment (1111), this imbalance is driven by SW cooling up to −90 W/m^2 (in 9 months) and is partially compensated by LW warming up to 40 W/m^2. The total (SW+LW) flux anomaly changes sign to positive 3 years after the eruption and the system starts to recover and to gain energy. At the surface (bottom of the atmosphere, BOA, bottom panel), reduced evaporation and positive latent heat flux anomaly up to 20 W/m^2 are the main mechanisms that drive the response, which offset strong SW cooling up to −70 W/m^2. The total energy flux anomaly at BOA also switches to a positive regime 3 years after the eruption.

Aerosols size distribution is among the primary controls on AOD and the lifetime of aerosols. AOD is responsible for the magnitude of radiative forcing, and aerosols lifetime controls the temporal extent of forcing. The evolution of aerosol size distribution modulates both of these parameters, and the corresponding climate effects have the same sign. A shift toward larger particles reduces AOD (per unit mass) in the visible (responsible for cooling) and increases AOD in longwave (responsible for warming) and results in a smaller overall radiative cooling. Larger particles also have a shorter lifetime with increasing size due to faster gravitational settling, which in turn results in weaker radiative cooling. In the case of size distribution represented by smaller particles, both effects work in the opposite direction. Figure 4 shows the evolution of the aerosols effective radius (top panel) and the contributions of the specific mechanisms (bottom panel) against the simulation with aerosol microphysics (1xxx). According to the reference experiment (1111), global mean effective radius peaks at 0.75 μm in 1.5 years and remains elevated for more than 10 years. This value can be compared with 0.5 μm observed (for a short period of time) after the Pinatubo eruption (Stenchikov

et al., 1998). The perturbations of effective radius (bottom panel) due to SO_2 and sulfate aerosols feedback are consistent with their effects on SO_2 oxidation. During the first year and a half, slower gas-to-particle conversion results in a lower number of nucleating particles, slower coagulation, and as a result up to 0.175 μm smaller effective radius. Since both feedback prolong SO_2 lifetime, the effective radius remains elevated after reaching the maximum. SO_2 feedback on dynamics causes the opposite effect on effective radius and facilitates gravitational removal of sulfate aerosols, resulting in smaller particles.

3.3. Climate Response

Thermal response in simulations largely follows radiative forcing. The top panel in Figure 5 shows that in the reference experiment the global mean sea surface temperature (SST) anomaly after the Toba eruption reaches the minimum of −5.5 K in 15–20 months and exceeds the level of natural variability for 7 years. The contribution (bottom panel) of aerosol microphysics (1xxx) reduces the magnitude of the anomaly by up to 100% and shortens development of the peak anomaly by about 2 years. The remaining second-order feedback each modulates SST cooling up to 0.5 K or up to 10% of the anomaly's largest magnitude. The aerosols (x1xx) and SO_2 (xx1x) feedback on photochemistry produce SST anomalies of similar magnitude and phase. These feedback cause warmer SST during the first 17 months and colder SST thereafter, consistent with their effect on AOD. The SO_2 greenhouse effect and feedback on dynamics (xxx1) contributes up to 0.7 K of SST anomaly and is equally important. The overall thermal effect of SO_2 feedbacks is represented by a less severe and shorter cooling anomaly. Similar diagnostics of surface air temperature (SAT) and precipitation are provided in the appendix.

3.4. Scaling of SO_2 Effects

In the previous sections we showed the importance of the SO_2 radiative effect for the selected size (Toba) of volcanic eruption. In this section we analyze scaling of the feedbacks and determine the threshold value of SO_2 emissions, below which SO_2 effects can be neglected. For this purpose we estimated SO_2 effect on photochemistry and radiative forcing for a range of plausible eruptions (1×, 10×, 100×, 1,000× Pinatubo) using stand-alone models. Technical details about the implementation of these tools and code availability are provided in Appendix A.

Figure 6 shows scaling of the ozone photolysis rate $J(O^1D)$ reduction due to SO_2 and sulfate aerosols. The calculations were done for the equatorial atmospheric profile using the stand-alone Line-By-Line Radiative Transfer Model (LBLRTM) coupled to the Discrete Ordinates Radiative Transfer Program for a Multi-Layered Plane-Parallel Medium (DISORT). Since the lifetime of the OH radical is short, the effect of $J(O^1D)$ reduction is only relevant for sulfate production in regions where SO_2 and O_3 profiles overlap (10–50 hPa in Figure 6). Additionally, O_3 and SO_2 layers are characterized by the largest absorption optical depth in UV (Figures A1 and A2), which causes rapid decay of the actinic flux profile. Thus, the SO_2 and O_3 overlap at 10 hPa (above the ozone maximum, Figure 6) is the region of the most intense SO_2 oxidation. It is also the region where relative changes of $J(O^1D)$ due to SO_2 and aerosols have the largest impact on chemistry. According to Figure 6, at the lower end of the scaling spectrum (1× Pinatubo) sulfate aerosols dominate and produce the largest relative changes of $J(O^1D)$ (in the photochemically active region). In this regime the lifetime of sulfate aerosols is also the longest, while the lifetime of SO_2 is shortest. Toward the 10×–100× Pinatubo range, SO_2 and aerosols effects become equally important. And for the stronger than Toba eruptions (1,000× Pinatubo), SO_2 effect dominates and starts to saturate. In this regime the lifetime of SO_2 is significantly enhanced, while the lifetime of sulfate aerosols is shortest.

According to Figure 6, at the lower end of the scaling spectrum (1× Pinatubo) both SO_2 and aerosols cause similar relative changes of $J(O^1D)$. In this regime the lifetime of sulfate aerosols is also much longer than that of SO_2, and thus their impact on photochemistry dominates. At the lower end of the scaling spectrum (1× Pinatubo), the reduction of $J(O^1D)$ is dominated by sulfate aerosols. Toward the 10×–100× Pinatubo range, SO_2 and aerosols effects become equally important. And for eruptions stronger than Toba (1,000× Pinatubo), the SO_2 effect dominates and starts to saturate.

Figure 7 shows the scaling of SO_2 radiative forcing. Radiative transfer calculations were done for the equatorial atmospheric profile using the stand-alone Rapid Radiative Transfer Model (RRTM, Appendix A). The total (SW+LW) SO_2 net radiative forcing at TOA is mostly represented by LW (greenhouse) warming. SW contribution due to enhanced absorption in UV is minor. Scaling of the SO_2 contribution to Earth's overall energy imbalance can be assessed by comparing radiative forcing obtained via RRTM calculations (Figure 7)

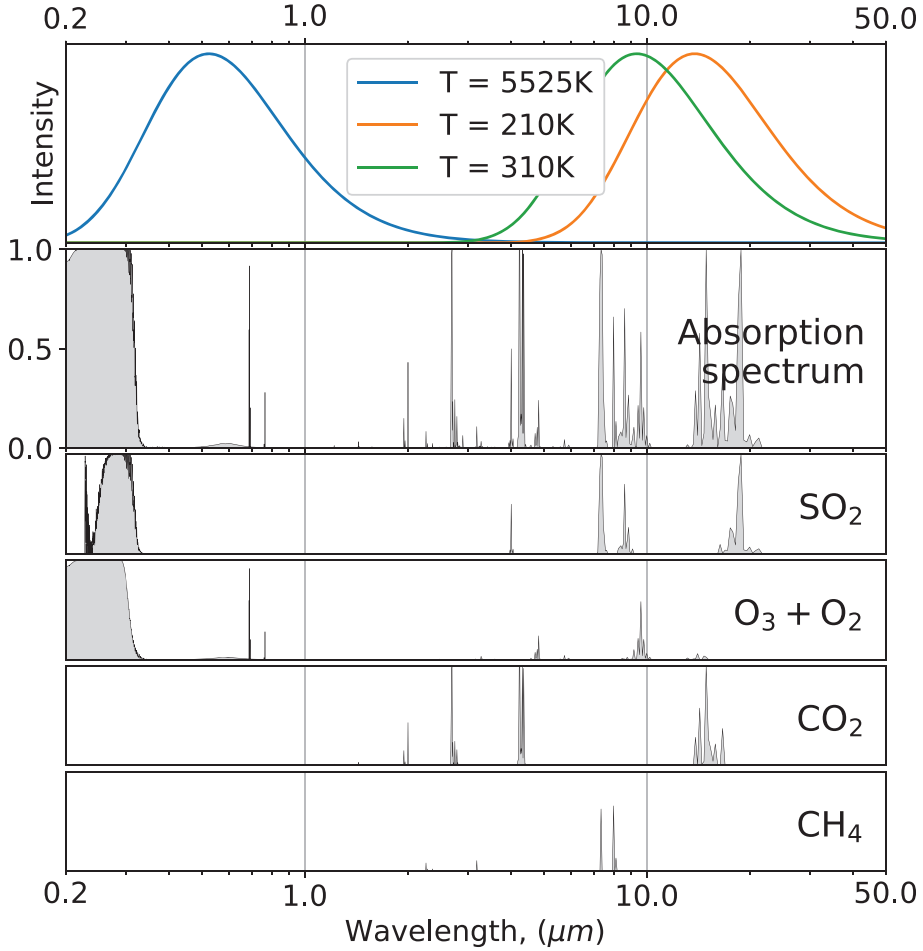

Figure A1. The line-by-line absorption spectrum for the realistic equatorial atmosphere between 10 and 50 hPa and the spectral intensities of the black body at the temperatures of the Sun, Earth surface, and tropopause. The uniform SO_2 mixing ratio of 10.9 ppmv (also 10–50 hPa) is included to represent the initial stage of the Toba eruption. Top panel shows the scaled (divided by the maximum value) spectral intensity of electromagnetic radiation emitted by a black body (Planck's law) at 5525 K, 310 K, and 210 K. Second panel shows the absorption spectra for the slab of atmosphere computed for all constituents. The remaining bottom panels show the absorption spectra computed for the individual major contributors in UV (O_3, O_2, SO_2) and LW (CO_2, and CH_4), respectively.

with global mean flux anomalies in ModelE (Figure 3), and in the case of the Pinatubo eruption, with the values published in Stenchikov et al. (1998).

After the Pinatubo eruption, the globally averaged LW net flux anomaly at TOA peaked at 2–3 W/m^2 (Soden et al., 2002; Stenchikov et al., 1998). The corresponding RRTM SO_2 radiative forcing (0.25 W/m^2) is 8–12 times smaller. Thus, SO_2 radiative effects can be neglected in the 1× Pinatubo case (since they are relatively short-lived). Toward the 100× Pinatubo (Toba) regime, relative contribution of SO_2 significantly increases and RRTM SO_2 greenhouse forcing (11.8 W/m^2) represents a considerable 30% of the peak LW energy imbalance at TOA (40 W/m^2) in the reference ModelE simulation (Figure 3).

Overall, according to Figures 6 and 7, the effects of a SO_2 mixing ratio of 0.1 ppmv (1× Pinatubo) are minor on the global scale from the photochemical and radiative forcing points of view. SO_2 effects scale up with the emitted mass and in the Toba regime are characterized by their pronounced magnitudes compared to the total. In addition to the large relative contribution, SO_2 lifetime also increases with the amount of emitted material, which prolongs the duration of the corresponding effects. During the initial stage of volcanic plume development, concentrations of emitted material can be several orders of magnitude higher locally. For example, after the Pinatubo eruption SO_2 peaked around 1–10 ppmv within the volcanic plume. Thus, 1× Pinatubo concentrations represent the transitional case, when SO_2 feedbacks should be considered to

properly capture the initial stage of volcanic plume evolution, but their impact on global climate is not strong enough.

4. Conclusions

Up to this point, the scientific community has proposed several mechanisms which have the potential to modulate volcanic winter effects and impact climate. As summarized in Table 1, previous studies of the Toba supereruption considered a limited subset of such mechanisms and targeted only on a single specific feedback. In this work we present an updated estimate of a Toba-sized volcanic eruption impact on climate. Our simulations for the first time include simultaneously the full set of the major mechanisms and their nonlinear interaction in the coupled ocean-atmosphere setup. Notably, SO_2 effects were for the first time evaluated in realistic interactive chemistry simulations coupled with aerosol microphysics.

We found that for the Toba case, the SO_2 radiative effect is as important as that of sulfate aerosols. It has a profound impact on sulfate chemistry, aerosols size distribution and optical properties, atmospheric dynamics, and climate response in general. The overall self-sustaining SO_2 effects are expressed by less severe, temporally more uniform, and shorter cooling of the Earth system. The main pathways of SO_2 impact are photochemistry, radiative forcing and atmospheric dynamics, all of which originate from the fact that SO_2 gas is optically active in several bands of the electromagnetic spectrum. Due to strong absorption in UV (in the spectral range similar to that of ozone), SO_2 perturbs photochemistry and modulates its climate impact. It reduces actinic flux, inhibits photolysis of ozone, and results in temporally more uniform distribution of sulfate AOD. As a greenhouse gas, SO_2 partially offsets sulfate aerosols cooling and mitigates Earth's energy imbalance. SO_2 impact on atmospheric heating rates is represented by the dipole structure (centered around the stratospheric ozone maximum), which causes lofting of the volcanic plume. In addition to the impact on atmospheric dynamics and transport, the enhanced rise of the volcanic plume boosts SO_2 potential to inhibit the chemistry, since its effects on actinic flux maximize at the altitudes of ozone maximum and above it.

The analysis of the scaling of SO_2 feedbacks shows that the corresponding effects become more prominent as the amount of emitted material increases. The lower threshold to consider these effects is represented by the Pinatubo-sized eruption and by local concentrations within the volcanic plume during the initial stage of its evolution. As the amount of emitted SO_2 grows the feedback on photochemistry becomes prominent on the global scale and sustains volcanic winter effects longer. In turn, the increased lifetime of SO_2 itself prolongs greenhouse warming and allows long-term lofting of the volcanic plume. To summarize, SO_2 represents an important additional agent responsible for the nonlinear scaling of the impact of volcanic eruptions on climate.

Appendix A: Stand-Alone LBLRTM, DISORT, and RRTM Models

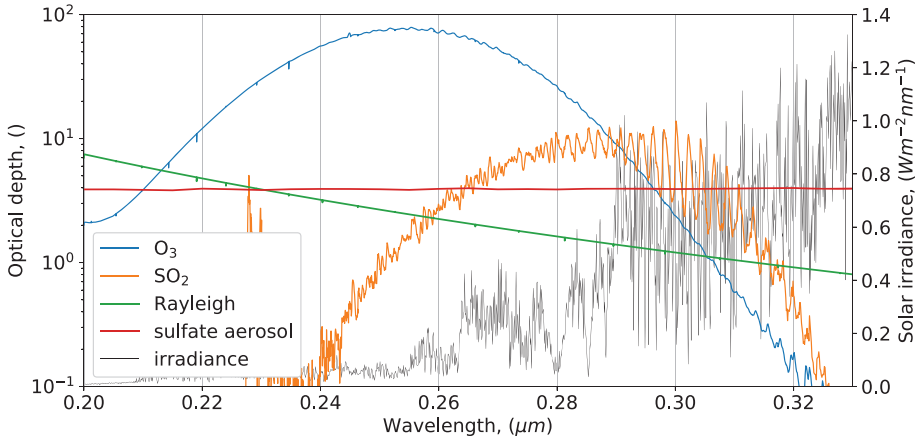

Figure A2. The line-by-line O_3, SO_2, Rayleigh, and sulfate aerosols column optical depths in UV for the realistic equatorial atmosphere. The corresponding O_3 and SO_2 profiles are shown in Figure 6. The uniform SO_2 mixing ratio of 10.9 ppmv (in the 10–50 hPa slab) is included to represent the initial stage of the Toba eruption. Sulfate aerosols size distribution is obtained from ModelE simulation of the Toba eruption and corresponds to the global mean AOD of 4.1 at 550 nm. The solar reference spectrum (gray, Chance & Kurucz, 2010) is plotted against the right vertical axis.

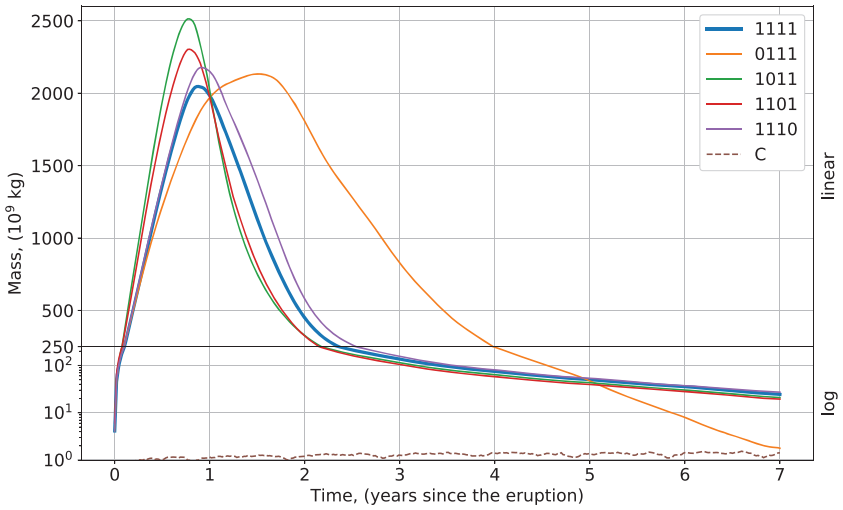

Figure A3. Instantaneous weekly globally integrated SO_4 mass for the reference experiment (1111, all feedback on), sensitivity experiments (xxxx, one of the feedback is switched off), and control experiment (C, does not include volcanic emissions). In the sensitivity experiments the following mechanisms are switched off one by one: aerosols microphysics (0111); feedback on photochemistry due to aerosols (1011) and SO_2 (1101); and SO_2 feedback on dynamics (1110). The linear-log threshold is equal to 250 Mt or 8.3% of the emitted mass (2,000 Mt * 96/64), where 96 and 64 are the molecular weights of SO_2 and SO_4, respectively.

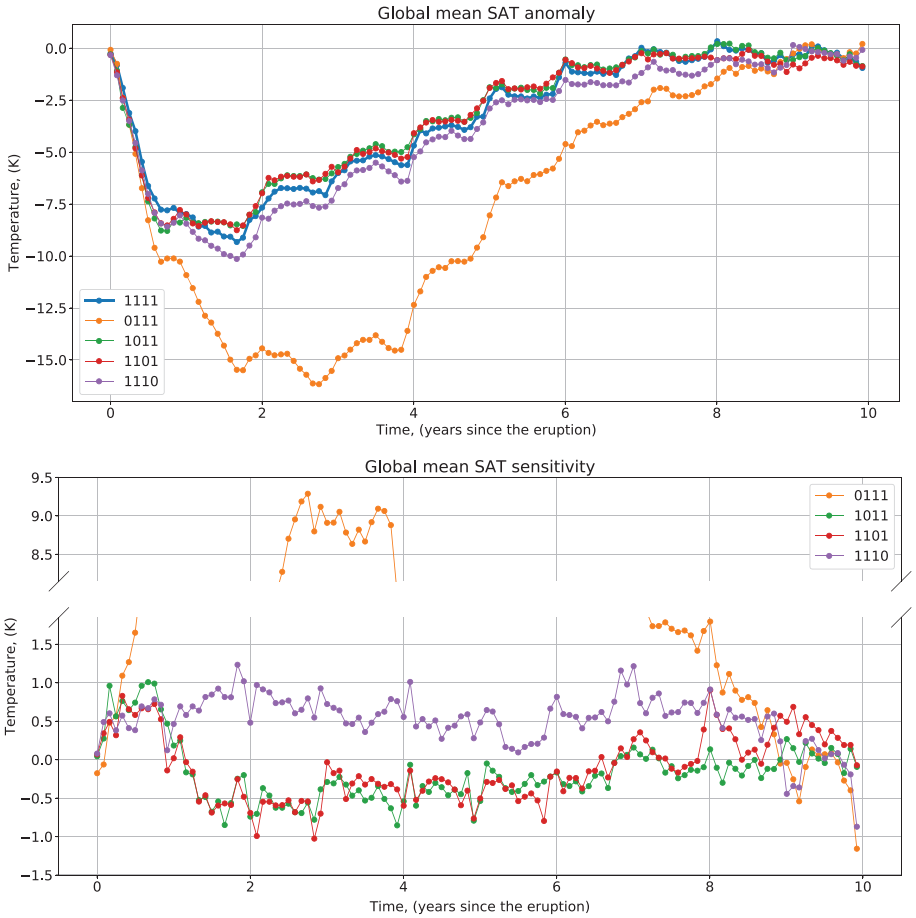

Figure A4. Same as Figure 5 but for surface air temperature.

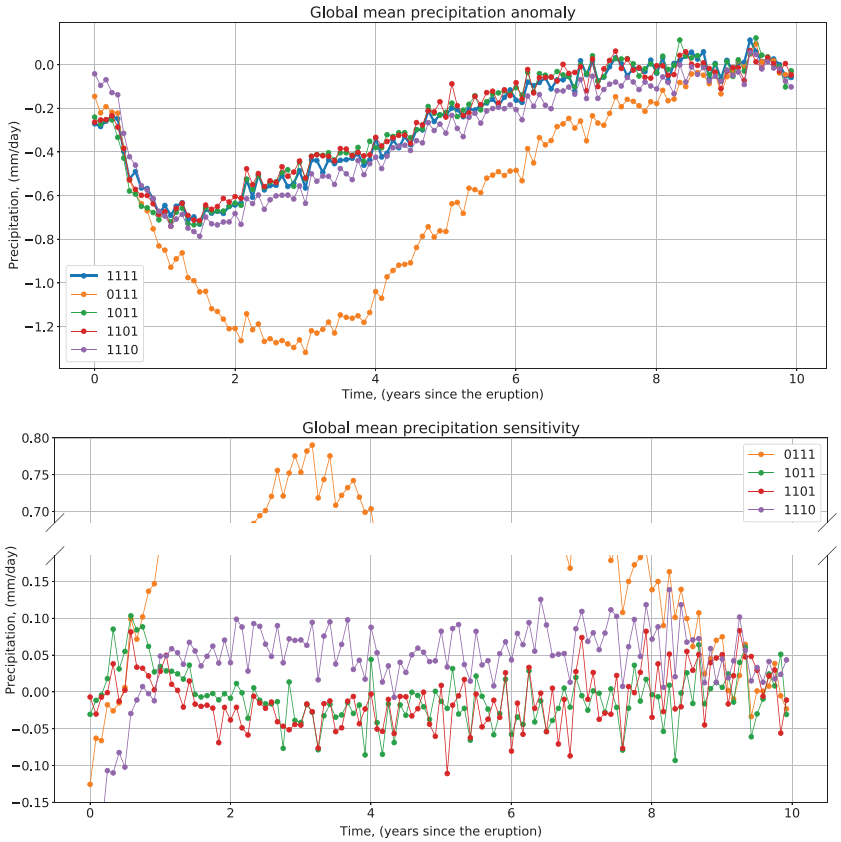

Figure A5. Same as Figure 5 but for precipitation.

Several stand-alone models were developed and employed to assess various SO_2 effects and to evaluate SO_2 implementation in ModelE. Gas absorption and scattering optical depths are computed using components from the LBLRTM (Clough et al., 1992, 2005). Sulfate aerosols optical properties (extinction, single scattering albedo, and phase function) are calculated for a given size distribution assuming the sphericity of particles using analytic Mie solution. Actinic fluxes in the atmosphere are computed using the DISORT (Stamnes et al., 1988) with the 16-stream setup. The chemical composition of the atmosphere is prescribed according to monthly climatology derived from the Global Modeling Initiative (GMI) model output. The GMI 3-D chemistry and transport model is integrated with meteorological fields from the Modern Era Retrospective-analysis for Research and Applications and includes full chemistry for both the troposphere and the stratosphere (Douglass et al., 1999; Strahan et al., 2011). Lower boundary conditions assume a Lambertian reflection with an ultraviolet surface albedo of 0.04. Photolysis rate calculations are based on the absorption cross section and quantum yield data recommended in Burkholder et al. (2015).

SO_2 radiative forcing and heating rates are computed using the same modeling framework but coupled to the stand-alone RRTM (Mlawer & Clough, 1997, 1998). The publicly available version of RRTM was improved to include the radiative effects of SO_2. A complete description of the modeling framework is given by Osipov et al. (2015) and the source code is publicly available at this site (https://github.com/SeregaOsipov/RRTM_ModelingFramework).

Additional diagnostics are provided in Figures A1–A10 and include the spectral optical properties of theatmosphere, globally integrated SO_4 mass, global mean SAT and precipitation, and the vertical profilesof the SO_2, SO_4, O_3, temperature and specific humidity.

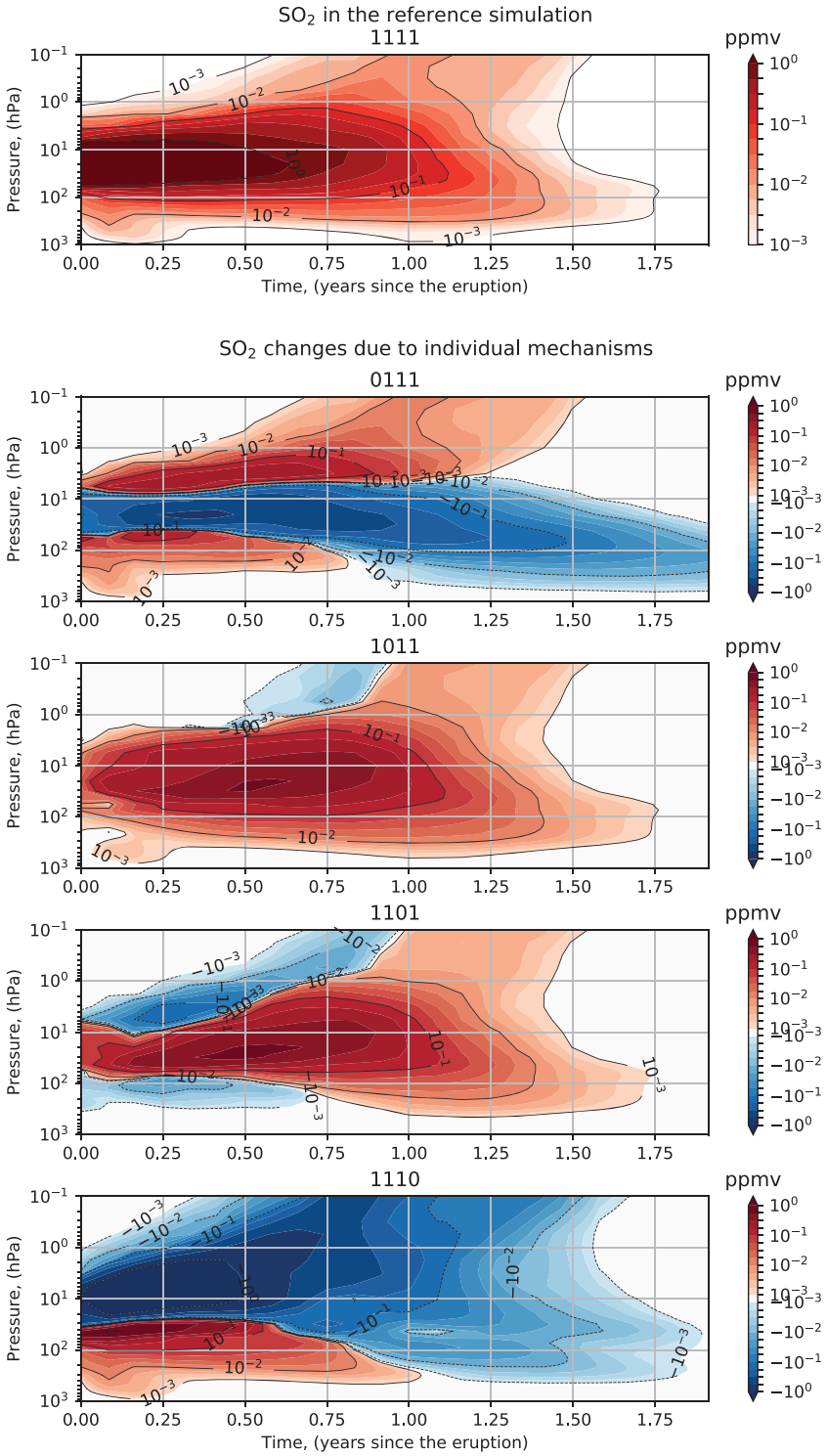

Figure A6. The monthly average global mean SO_2 profiles and contribution of the individual feedbacks. Top panel shows SO_2 for the reference experiment (1111, all feedback are on). The remaining panels show SO_2 changes due to individual mechanisms, represented by the difference between reference and sensitivity simulations (xxxx, one of the feedback is switched off). In sensitivity experiments the following mechanisms are switched off one by one: aerosols microphysics (0111); feedback on photochemistry due to aerosols (1011) and SO_2 (1101); and SO_2 feedback on dynamics (1110).

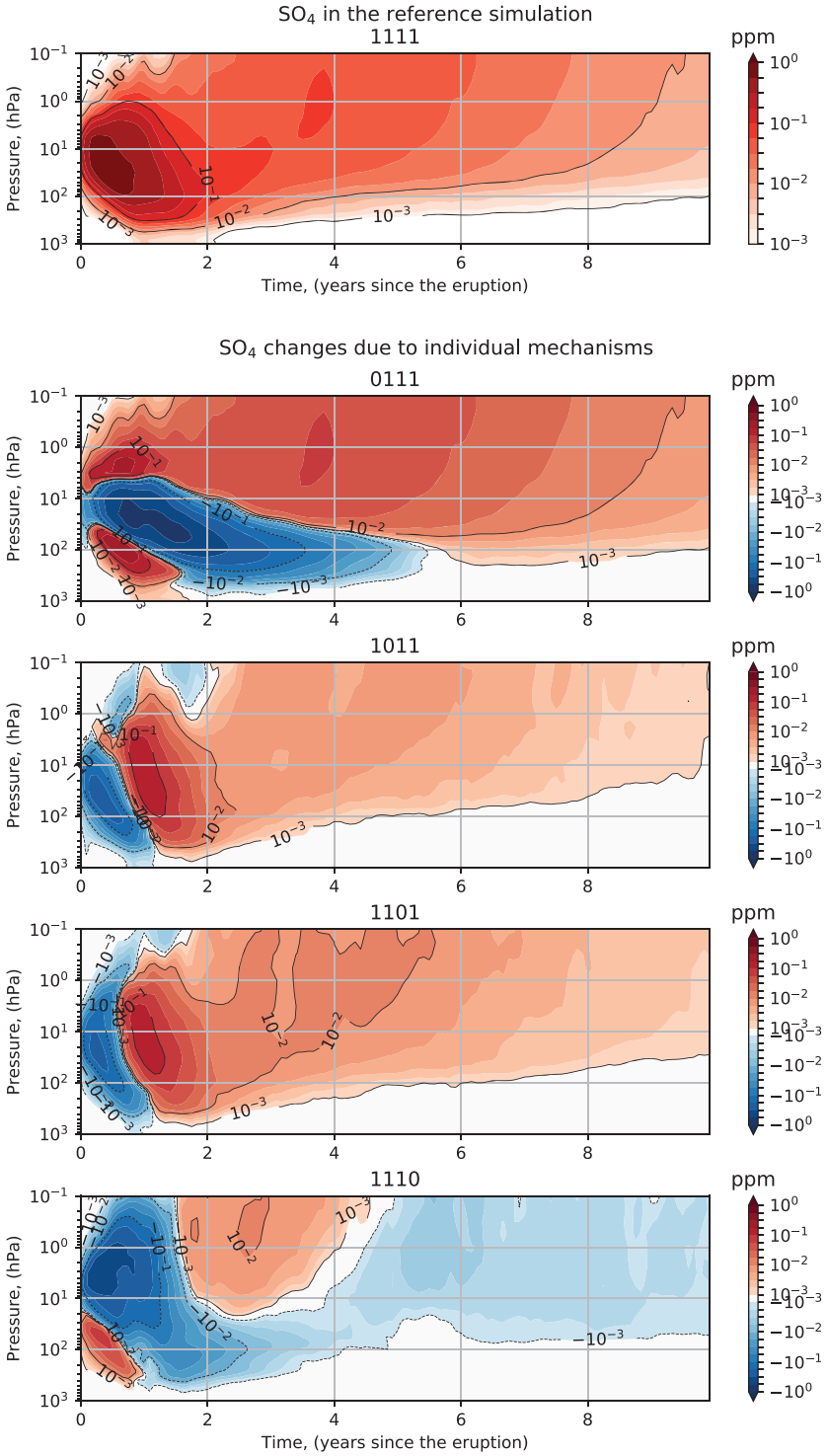

Figure A7. Same as Figure A6 but for SO_4.

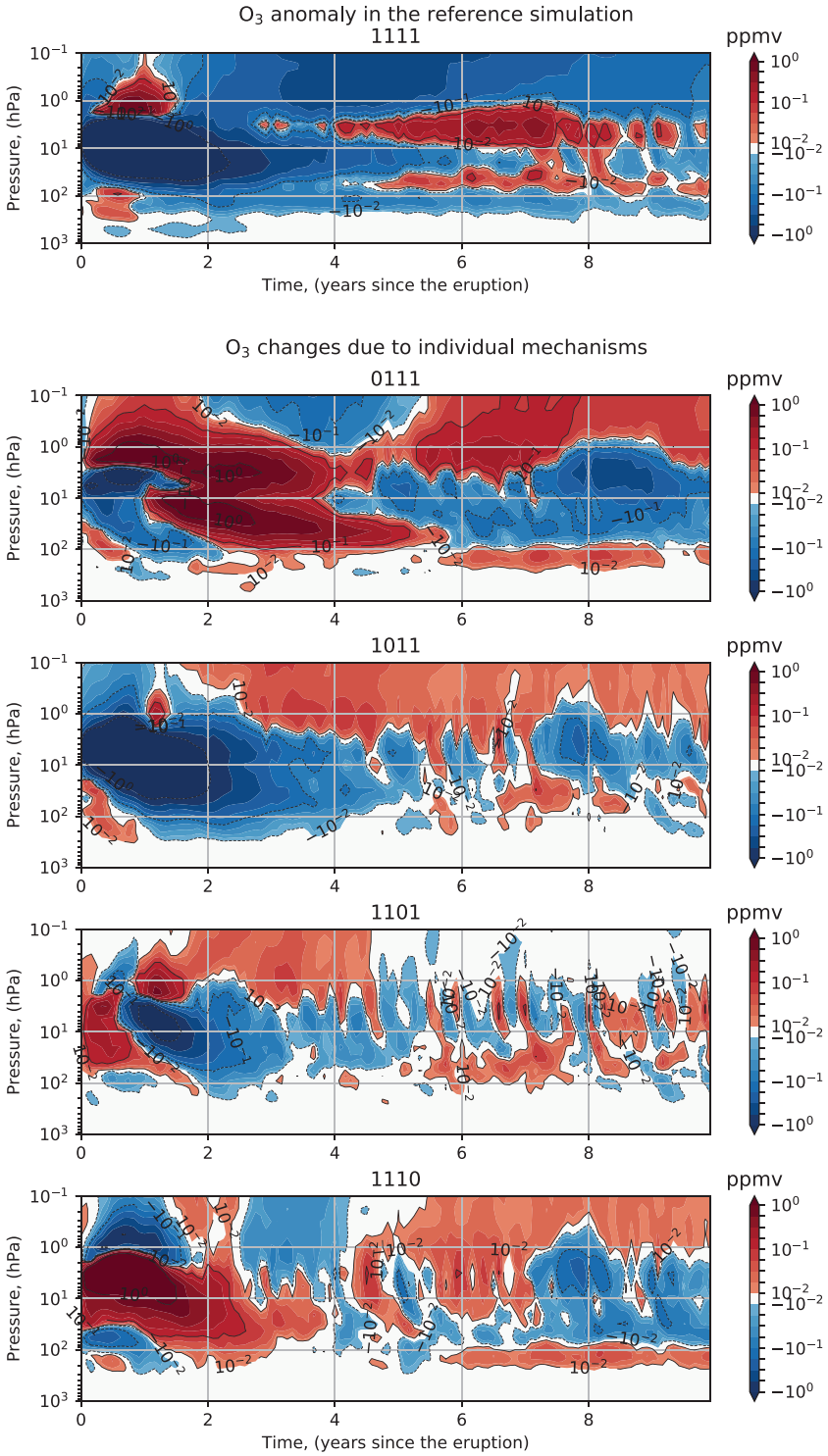

Figure A8. Same as Figure A6 but for O_3, and top panel shows anomalies of the reference simulation (1111, with the SO_2 emissions) with respect to the control run (C, without SO_2 emissions).

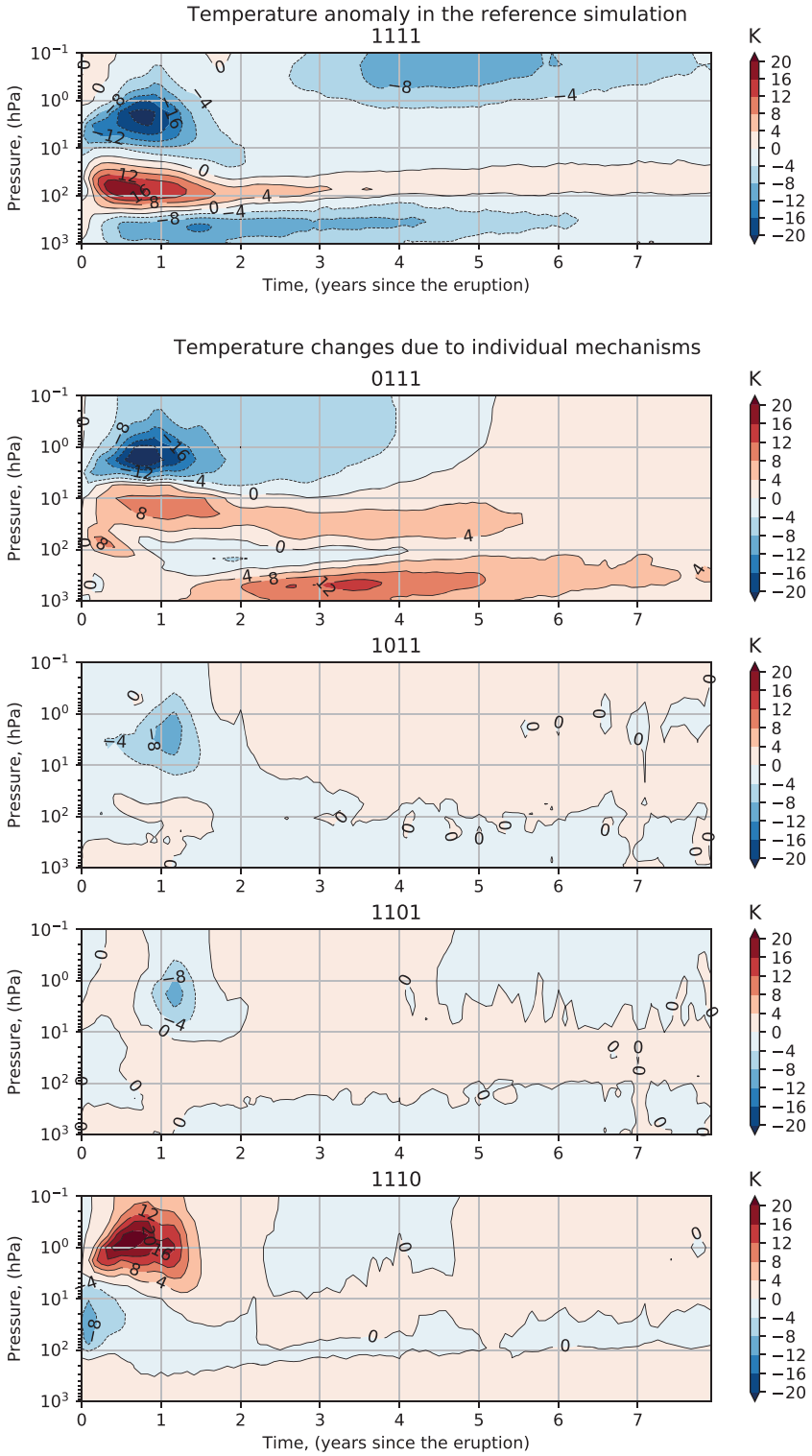

Figure A9. Same as Figure A6 but for temperature, and top panel shows anomalies of the reference simulation (1111, with the SO_2 emissions) with respect to the control run (C, without SO_2 emissions).

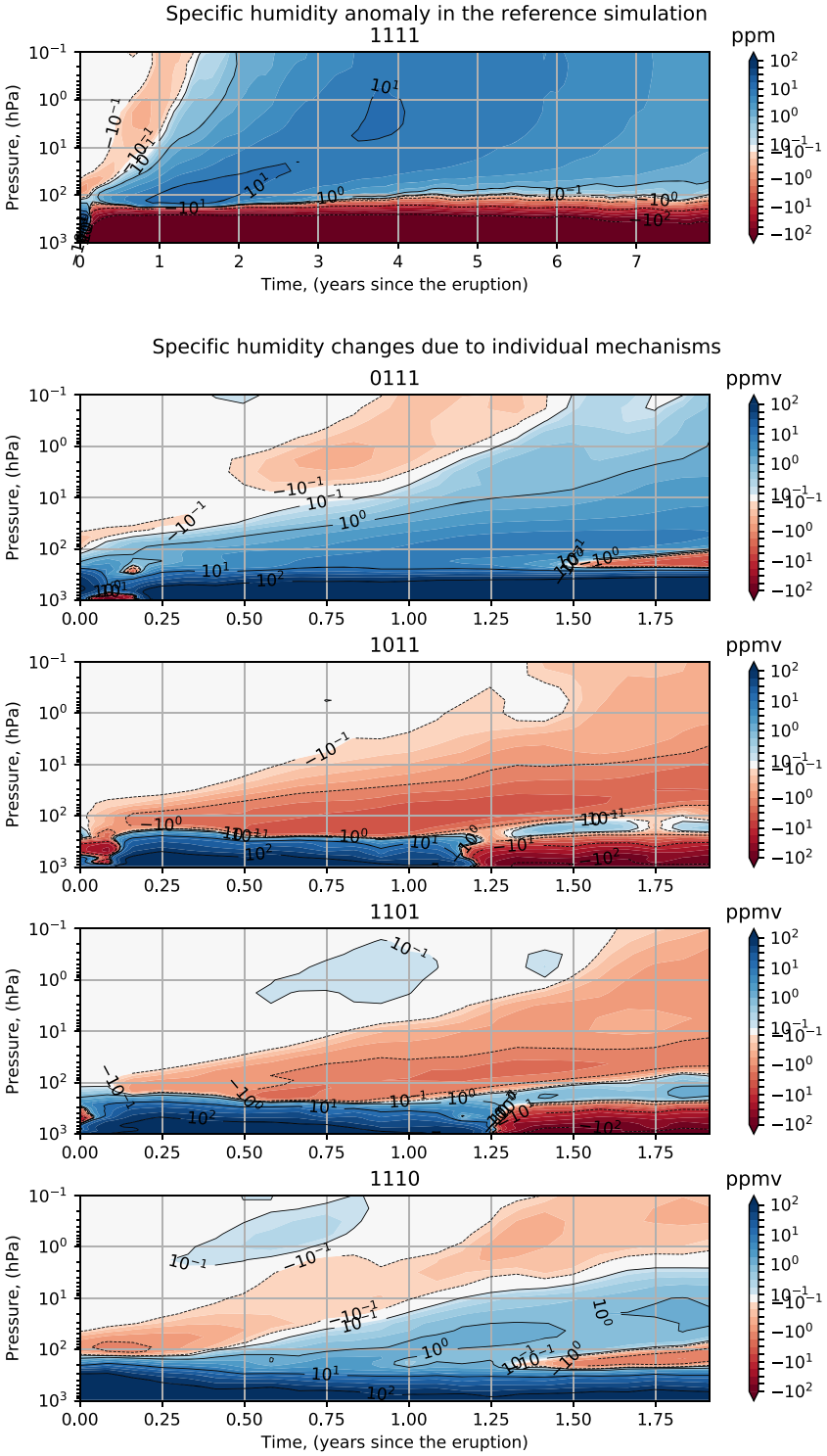

Figure A10. Same as Figure A6 but for specific humidity, and top panel shows anomalies of the reference simulation (1111, with the SO_2 emissions) with respect to the control run (C, without SO_2 emissions).

Acknowledgments
The research reported in this publication was supported by funding from King Abdullah University of Science and Technology (KAUST). We thank the KAUST Supercomputing Laboratory for providing computer resources. We thank Karen Cady-Pereira, Eli Mlawer, and Mike Iacono from Atmospheric and Environmental Research (AER) for their help in adding SO_2 radiative effects into the RRTM, RRTMG stand-alone models, and RRTMG radiation modules for the Weather Research and Forecasting (WRF) model. The ERA-Interim data were obtained from the ECMWF Data Server with 0.75° by 0.75° horizontal and 6 hr temporal resolution. The modeling framework and other data necessary to reproduce the simulations are publicly available through KAUST Repository (http://hdl.handle.net/10754/655974). K. T. and S. E. B. acknowledge support from NASA ACMAP (Atmospheric Composition Modeling and Analysis Program) Contract NNX15AE36G. A. N. L. and S. E. B. thank NASA GISS for institutional support.

References

Ambrose, S. H. (1998). Late pleistocene human population bottlenecks, volcanic winter, and differentiation of modern humans. *Journal of Human Evolution*, *34*(6), 623–651. https://doi.org/10.1006/jhev.1998.0219

Bauer, S. E., Wright, D. L., Koch, D., Lewis, E. R., McGraw, R., Chang, L.-S., et al. (2008). Matrix (multiconfiguration aerosol tracker of mixing state): An aerosol microphysical module for global atmospheric models. *Atmospheric Chemistry and Physics*, *8*(20), 6003–6035. https://doi.org/10.5194/acp-8-6003-2008

Bekki, S. (1995). Oxidation of volcanic SO_2: A sink for stratospheric oh and h2o. *Geophysical Research Letters*, *22*(8), 913–916. https://doi.org/10.1029/95GL00534

Bekki, S., Pyle, J. A., Zhong, W., Toumi, R., Haigh, J. D., & Pyle, D. M. (1996). The role of microphysical and chemical processes in prolonging the climate forcing of the Toba eruption. *Geophysical Research Letters*, *23*(19), 2669–2672. https://doi.org/10.1029/96GL02088

Burkholder, J., Sander, S., Abbatt, J., Barker, J., Huie, R., Kolb, C., et al. (2015). Chemical kinetics and photochemical data for use in atmospheric studies. *Evaluation*, *18*, 15–10.

Chance, K., & Kurucz, R. L. (2010). An improved high-resolution solar reference spectrum for earth's atmosphere measurements in the ultraviolet, visible, and near infrared. *Journal of Quantitative Spectroscopy and Radiative Transfer*, *111*(9), 1289–1295. https://doi.org/10.1016/j.jqsrt.2010.01.036,Special Issue Dedicated to Laurence S. Rothman on the Occasion of his 70th Birthday.

Clough, S. A., Iacono, M. J., & Moncet, J.-L. (1992). Line-by-line calculations of atmospheric fluxes and cooling rates: Application to water vapor. *Journal of Geophysical Research*, *97*(D14), 15,761–15,785. https://doi.org/10.1029/92JD01419

Clough, S. A., Shephard, M. W., Mlawer, E. J., Delamere, J. S., Iacono, M. J., Cady-Pereira, K., et al. (2005). Atmospheric radiative transfer modeling: A summary of the {AER} codes. *Journal of Quantitative Spectroscopy and Radiative Transfer*, *91*(2), 233–244. https://doi.org/10.1016/j.jqsrt.2004.05.058

Dickerson, R. R., Kondragunta, S., Stenchikov, G., Civerolo, K. L., Doddridge, B. G., & Holben, B. N. (1997). The impact of aerosols on solar ultraviolet radiation and photochemical smog. *Science*, *278*(5339), 827–830. https://doi.org/10.1126/science.278.5339.827

Douglass, A., Prather, M., Hall, T., Strahan, S., Rasch, P., Sparling, L., et al. (1999). Choosing meteorological input for the global modeling initiative assessment of high-speed aircraft. *Journal of Geophysical Research*, *104*(D22), 27,545–27,564.

English, J. M., Toon, O. B., & Mills, M. J. (2013). Microphysical simulations of large volcanic eruptions: Pinatubo and Toba. *Journal of Geophysical Research*, *118*, 1880–1895. https://doi.org/10.1002/jgrd.50196

Guo, S., Bluth, G. J. S., Rose, W. I., Watson, I. M., & Prata, A. J. (2004). Re-evaluation of SO_2 release of the 15 June 1991 Pinatubo eruption using ultraviolet and infrared satellite sensors. *Geochemistry, Geophysics, Geosystems*, *5*, Q04001. https://doi.org/10.1029/2003GC000654

Jones, G. S., Gregory, J. M., Stott, P. A., Tett, S. F. B., & Thorpe, R. B. (2005). An AOGCM simulation of the climate response to a volcanic super-eruption. *Climate Dynamics*, *25*(7), 725–738. https://doi.org/10.1007/s00382-005-0066-8

Koch, D., Jacob, D., Tegen, I., Rind, D., & Chin, M. (1999). Tropospheric sulfur simulation and sulfate direct radiative forcing in the Goddard Institute for space studies general circulation model. *Journal of Geophysical Research*, *104*(D19), 23,799–23,822. https://doi.org/10.1029/1999JD900248

Koch, D., Schmidt, G. A., & Field, C. V. (2006). Sulfur, sea salt, and radionuclide aerosols in GISS ModelE. *Journal of Geophysical Research*, *111*, D06206. https://doi.org/10.1029/2004JD005550

Kondratyev, K. Y., Moskalenko, N. I., & Parzhin, S. N. (1986). A comparative analysis of the volcanic impact on the climates of the Earth and Mars. *Earth, Moon, and Planets*, *35*(1), 13–18. https://doi.org/10.1007/BF00054131

Lacis, A., Hansen, J., & Sato, M. (1992). Climate forcing by stratospheric aerosols. *Geophysical Research Letters*, *19*(15), 1607–1610. https://doi.org/10.1029/92GL01620

Lane, C. S., Chorn, B. T., & Johnson, T. C. (2013). Ash from the Toba supereruption in Lake Malawi shows no volcanic winter in East Africa at 75 ka. *Proceedings of the National Academy of Sciences of the United States of America*, *110*, 8025–8029.

Lary, D. J., Balluch, M., & Bekki, S. (1994). Solar heating rates after a volcanic eruption: The importance of SO_2 absorption. *Quarterly Journal of the Royal Meteorological Society*, *120*(520), 1683–1688. https://doi.org/10.1002/qj.49712052011

LeGrande, A. N., Tsigaridis, K., & Bauer, S. E. (2016). Role of atmospheric chemistry in the climate impacts of stratospheric volcanic injections. *Nature Geoscience*, *9*(9), 652–655. https://doi.org/10.1038/ngeo2771

Mlawer, E., & Clough, S. (1997). On the extension of rapid radiative transfer model to the shortwave region. In *Proceedings of the sixth atmospheric radiation measurement (arm) science team meeting, march 4-7, 1996, san antonio, texas, conf-9603149, u.s. dept. of energy, washington, dc, 1997*, pp. 223–226.

Mlawer, E., & Clough, S. (1998). Shortwave and longwave enhancements in the rapid radiative transfer model. In *Proceedings of the 7th atmospheric radiation measurement (arm) science team meeting*.

Oppenheimer, C. (2002). Limited global change due to the largest known Quaternary eruption, Toba ≈74 kyr BP? *Quaternary Science Reviews*, *21*(14), 1593–1609. https://doi.org/10.1016/S0277-3791(01)00154-8

Osipov, S., Stenchikov, G., Brindley, H., & Banks, J. (2015). Diurnal cycle of the dust instantaneous direct radiative forcing over the Arabian Peninsula. *Atmospheric Chemistry and Physics*, *15*(16), 9537–9553. https://doi.org/10.5194/acp-15-9537-2015

Pinto, J. P., Turco, R. P., & Toon, O. B. (1989). Self-limiting physical and chemical effects in volcanic eruption clouds. *Journal of Geophysical Research: Atmospheres*, *94*(D8), 11,165–11,174. https://doi.org/10.1029/JD094iD08p11165

Rampino, M. R., & Self, S. (1992). Volcanic winter and accelerated glaciation following the Toba super-eruption. *Nature*, *359*, 50–52. https://doi.org/10.1038/359050a0

Robock, A. (2000). Volcanic eruptions and climate. *Reviews of Geophysics*, *38*(2), 191–219. https://doi.org/10.1029/1998RG000054

Robock, A., Ammann, C. M., Oman, L., Shindell, D., Levis, S., & Stenchikov, G. (2009). Did the Toba volcanic eruption of 74 ka b.p. produce widespread glaciation? *Journal of Geophysical Research*, *114*, D10107. https://doi.org/10.1029/2008JD011652

Russell, G. L., Miller, J. R., & Rind, D. (1995). A coupled atmosphere ocean model for transient climate change studies. *Atmosphere-Ocean*, *33*(4), 683–730. https://doi.org/10.1080/07055900.1995.9649550

Sato, M., Hansen, J. E., McCormick, M. Patrick, & Pollack, J. B. (1993). Stratospheric aerosol optical depths, 1850-1990. *Journal of Geophysical Research*, *98*(D12), 22,987–22,994. https://doi.org/10.1029/93JD02553

Schmidt, G. A., Kelley, M., Nazarenko, L., Ruedy, R., Russell, G. L., Aleinov, I., et al. (2014). Configuration and assessment of the GISS ModelE2 contributions to the CMIP5 archive. *Journal of Advances in Modeling Earth Systems*, *6*, 141–184. https://doi.org/10.1002/2013MS000265

Schmidt, G. A., Ruedy, R., Hansen, J. E., Aleinov, I., Bell, N., Bauer, M., et al. (2006). Present-day atmospheric simulations using GISS ModelE: Comparison to in situ, satellite, and reanalysis data. *Journal of Climate*, *19*(2), 153–192. https://doi.org/10.1175/JCLI3612.1

Shindell, D. T., Pechony, O., Voulgarakis, A., Faluvegi, G., Nazarenko, L., Lamarque, J.-F., et al. (2013). Interactive ozone and methane chemistry in GISS-E2 historical and future climate simulations. *Atmospheric Chemistry and Physics*, *13*(5), 2653–2689. https://doi.org/10.5194/acp-13-2653-2013

Smith, E. I., Jacobs, Z., Johnsen, R., Ren, M., Fisher, E. C., Oestmo, S., et al. (2018). Humans thrived in South Africa through the Toba eruption about 74,000 years ago. *Nature*, *555*, 511–515. https://doi.org/10.1038/nature25967

Soden, B. J., Wetherald, R. T., Stenchikov, G. L., & Robock, A. (2002). Global cooling after the eruption of Mount Pinatubo: A test of climate feedback by water vapor. *Science*, *296*(5568), 727–730. https://doi.org/10.1126/science.296.5568.727

Stamnes, K., Tsay, S.-C., Wiscombe, W., & Jayaweera, K. (1988). Numerically stable algorithm for discrete-ordinate-method radiative transfer in multiple scattering and emitting layered media. *Applied Optics*, *27*(12), 2502–2509. https://doi.org/10.1364/AO.27.002502

Stenchikov, G., Delworth, T. L., Ramaswamy, V., Stouffer, R. J., Wittenberg, A., & Zeng, F. (2009). Volcanic signals in oceans. *Journal of Geophysical Research*, *114*, D16104. https://doi.org/10.1029/2008JD011673

Stenchikov, G. L., Kirchner, I., Robock, A., Graf, H.-F., Antuna, J. C., Grainger, R., et al. (1998). Radiative forcing from the 1991 Mount Pinatubo volcanic eruption. *Journal of Geophysical Research*, *103*(D12), 13,837–13,857.

Strahan, S. E., Douglass, A. R., Stolarski, R. S., Akiyoshi, H., Bekki, S., Braesicke, P., et al. (2011). Using transport diagnostics to understand chemistry climate model ozone simulations. *Journal of Geophysical Research*, *116*, D17302. https://doi.org/10.1029/2010JD015360

Timmreck, C., Graf, H.-F., Lorenz, S. J., Niemeier, U., Zanchettin, D., Matei, D., et al. (2010). Aerosol size confines climate response to volcanic super-eruptions. *Geophysical Research Letters*, *37*, L24705. https://doi.org/10.1029/2010GL045464

Timmreck, C., Graf, H.-F., Zanchettin, D., Hagemann, S., Kleinen, T., & Krger, K. (2012). Climate response to the Toba super-eruption: Regional changes. *Quaternary International*, *258*, 30–44. https://doi.org/10.1016/j.quaint.2011.10.008, The Toba Volcanic Super-eruption of 74,000 Years Ago: Climate Change, Environments, and Evolving Humans. ,

Ward, P. L. (2009). Sulfur dioxide initiates global climate change in four ways. *Thin Solid Films*, *517*(11), 3188–3203. https://doi.org/10.1016/j.tsf.2009.01.005

Wild, O., Zhu, X., & Prather, M. J. (2000). Fast-J: Accurate simulation of in- and below-cloud photolysis in tropospheric chemical models. *Journal of Atmospheric Chemistry*, *37*(3), 245–282. https://doi.org/10.1023/A:1006415919030

Yost, C. L., Jackson, L. J., Stone, J. R., & Cohen, A. S. (2018). Subdecadal phytolith and charcoal records from Lake Malawi, East Africa imply minimal effects on human evolution from the 74 ka Toba supereruption. *Journal of Human Evolution*, *116*, 75–94. https://doi.org/10.1016/j.jhevol.2017.11.005

Zhong, W., Haigh, J. D., Toumi, R., & Bekki, S. (1996). Infrared heating rates in the stratosphere due to volcanic sulphur dioxide. *Quarterly Journal of the Royal Meteorological Society*, *122*(534), 1459–1466. https://doi.org/10.1002/qj.49712253411